# EFFECT OF TINE FURROW OPENER ON SOIL MOVEMENT LAWS USING THE DISCRETE ELEMENT METHOD AND SOIL BIN STUDY

/

# 基于 EDEM 仿真与土槽试验的移动式开沟器土壤扰动规律研究

**Chengyou SONG[1)], Xiangcai ZHANG[*1)], Hui LI[2)], Yuchun LV[1)], Yonggang LI[1)], Xianliang WANG[1)], Zhongcai WEI[1)], Xiupei CHENG[1)]**

[1)]School of Agricultural and Food Science, Shandong University of Technology, Zibo (255000), China;
[2)]Shandong Academy of Agricultural Machinery Sciences, Jinan (250010), China
*Tel: +86-15169235925; E-mail: zxcai0216@163.com*
*Corresponding author: Xiangcai Zhang*
*DOI: https://doi.org/10.35633/inmateh-68-35*

***Keywords:*** *tine furrow opener, discrete element, soil disturbance, high-speed photography*

## ABSTRACT

*The mechanism of furrow opener-soil interaction plays an important role in analyzing the process of no-till planting furrow opener. In order to study the disturbance effect of the furrow opener on the loam soil, firstly, the three-dimensional model of the furrow opener was established by using SolidWorks. Secondly, the 3D discrete element model of furrow opener-soil interaction was established by EDEM software. Combined with the indoor soil bin test bench and high-speed camera technology, the micro-disturbance and macro-disturbance behavior of the furrow opener on soil at different positions, speeds and operating depths were compared and analyzed. The results showed that, the disturbance range of soil was decreased with the increase of the distance between the furrow opener and the soil. At different locations, the disturbance range of soil from large to small was the surface layer, the shallow layer and the middle layer. Under the conditions of three different layouts of furrow openers, through the comparison of the soil trench test and the simulation test, it was determined that the furrow openers in a staggered layout would be beneficial to reduce the degree of soil disturbance. In the trenching process, the soil movement velocity was decreased with the increase of the distance between the soil and the furrow opener, and the distribution curves of the same-speed soil particles were basically consistent with the curves of the furrow opener. The average velocities of soil particles with different velocities and depths in different directions were the surface layer, the shallow layer and the middle layer. However, there were differences in the maximum velocities of soil particles in different directions. By comparing the data obtained from the simulation test and the soil bin test, it was found that the parameters obtained from the simulation and the test were basically consistent, and it was determined that the discrete element simulation could simulate the soil disturbance behavior of the furrow opener more accurately. The relative errors of cross-sectional area of the front furrow opener and the rear furrow opener were 2.48 % and 5.2 %, respectively. The relative errors of the dynamic soil rate of the front furrow opener and the rear furrow opener were 0.25 % and 5.12 %, respectively.*

## 摘要

*开沟器—土壤之间的相互作用机理对于分析开沟器的免耕作业过程有着重要的作用。为研究开沟器对土壤的扰动作用，首先利用 SolidWorks 建立开沟器三维模型；其次使用 EDEM 软件建立开沟器-土壤相互作用的三维离散元模型。结合室内土槽试验台以及高速摄像技术，对比分析不同位置、不同速度、不同作业深度下开沟器对土壤的微观扰动以及宏观扰动行为。结果表明，土壤的扰动范围会随着与开沟器之间距离的增大而逐渐减小；不同位置土壤的扰动范围由大到小依此为表层、浅层、中层。在开沟器 3 种不同布局方式的条件下，通过对土槽试验和仿真试验的对比，确定开沟器以相互交错的布局方式，会有利于减小土壤的扰动程度。在开沟过程中，土壤的运动速度会随着与开沟器之间距离的增大而逐渐减小，土壤颗粒的等速度分布曲线与开沟器的切土刃口弧线基本吻合；不同速度、不同深度的土壤颗粒在不同方向上的平均速度由大到小均为表层、浅层、中层；但土壤颗粒在不同方向上的最大速度存在着差异。通过对仿真试验与土槽试验获得的数据进行对比，发现仿真与试验获取的各项参数基本一致，确定离散元仿真能够较准确的模拟开沟器对土壤的扰动行为；前排开沟器和后排开沟器的沟型截面积相对误差分别为 2.48%、5.2%，前排开沟器和后排开沟器的动土率相对误差分别为 0.25%、5.12%。*

## INTRODUCTION

As the key tillage component of no-tillage drill *(Zhang et al., 2016)*, furrow opener is conducive to forming a good seedbed environment. At the same time, the tine furrow opener is an important ditching component in the process of sowing and trenching. Soil disturbance process has always been a complex process, which is mainly affected by the difference of soil spatial distribution, the dynamics of tillage components, and the movement and breakage of soil itself *(Fang et al., 2016; Fang et al., 2016)*. Therefore, it is extremely difficult to analyze the behavior of furrow opener on soil disturbance. And the traditional test method cannot accurately describe the micro-disturbance movement of soil caused by the furrow opener during the tillage process.

In recent years, researchers have mainly analyzed soil-tillage component interactions through simulation software. At present, the main methods commonly used include finite element method (FEM) and discrete element method (DEM). The finite element method (FEM) studies the material as a continuum, but it is difficult to simulate the disturbance behavior of soil and the interaction between the soil and the furrow opener *(Abo-Elnor et al., 2004; Fielke, 1999; Tagar et al., 2015)*. The discrete element method (DEM) can be used to simulate the *macroscopic and microscopic* deformation of granular objects and research materials, allowing the formation and destruction of contact between granular materials *(Huang et al., 2016)*. Domestic and foreign scholars have conducted extensive research on the operating characteristics of furrow openers based on discrete element method (DEM) *(Barr et al., 2020; Chen et al., 2013; Matin et al., 2014; Ucgul et al., 2015; Ucgul et al., 2017; Wang et al., 2021; Wang et al., 2022; Zhang et al., 2007)*. For example, *Yu et al., (2009),* used the DEM to study the opening process of the furrow opener, analyzed the working resistance of the furrow opener under different conditions, and proved the feasibility of using the discrete element method (DEM) to analyze the operating process of the furrow opener by comparing the actual test results with the simulation results. *Ucgul et al. (2014)* used different discrete element contact models to simulate the furrow opener in the case of non-cohesive soil and cohesive soil respectively, and verified the reliability of the discrete element method (DEM). By using the discrete element method (DEM), *Gou et al. (2012)* found that when the operating depth was fixed, with the increase of operating speed, the vertical force of the furrow opener increased slightly, while the horizontal working resistance increased greatly. Through the discrete element simulation, *Liu et al. (2021)* determined that under the condition of a certain width of the furrow opener, with the increase of the sowing depth and the angle of penetration, the working resistance was on the rise, and the angle of penetration had the greatest influence on the working resistance. Under the condition of a certain angle of penetration or sowing depth, with the increase of the width of the furrow opener, the working resistance did not change significantly. Through simulation, *Zhao et al. (2017)* determined that the working resistance of the furrow opener increased with the increase of soil moisture content under a certain depth, and the change of soil disturbance by the furrow opener was not obvious under the condition of constant depth and moisture content. The existing researches mainly focused on the macro-disturbance behavior of soil and the effects of individual furrow opener on soil, but there lacks the exploration of micro-disturbance behavior of soil under different conditions, also the law of soil disturbance and the interaction effect of tine furrow openers need further study.

Therefore, the objective of this study was to analyze the disturbance behavior of the farmland soil by the tine furrow opener, and the soil bin test bench was used to carry out the ditching test with the comprehensive utilization of DEM and high-speed camera during the tillage process. It focused on the study of the disturbance process of seedbed and the interaction effects between adjacent furrow openers. The micro-disturbance movement and macro-disturbance behavior of the soil was also analyzed under different operating conditions (different furrow depths, different operating speeds, different position relationship of furrow openers and different layout method), that can provide experimental basis for the design and optimization of the structure of the furrow opener and the layout of the tine furrow opener.

## MATERIALS AND METHODS

### Description of tine furrow opener

As the soil touching parts, the tine furrow opener directly comes in contact with the soil, and the structure parameters of the furrow opener affects the seedbed environment during the seeding operation. Rake angle (α) and penetration clearance angle (β) were the main operating parameters. The researches showed that the rake angle (α), edge of tine furrow opener and the ground surface, will raise the soil layer and go against the operation of inserting into the soil when the rake angle is too large, will make the shovel tip of the furrow opener too long and reduce the strength when the rake angle is too small *(Jia et al., 2020; Liu et al., 2021; Manuwa et al., 2012; Singh et al., 2016; Ucgul et al., 2014; Yao et al., 2009)*. The penetration clearance angle (β),

between the bottom of the furrow opener and the ground surface, will affect the quality of backfilling soil when the angle is too large, and the small angle will reduce the penetration performance *(Jia et al., 2020; Zhang et al., 2016)*. Therefore, the tine furrow opener, shown in Fig. 1, was designed as the test part to analyze its effects on soil disturbance, and its structure diagram was shown in Fig. 1. The height of the furrow opener (h) was 540 mm, the length of the shovel handle (L) was 100 mm, the width of the furrow opener (d) was 40 mm *(Zhang et al., 2016)*, the rake angle (α) was 55° *(Yao et al., 2009)*, and the penetration clearance angle (β) was 5°.*(Wang et al., 2021)*

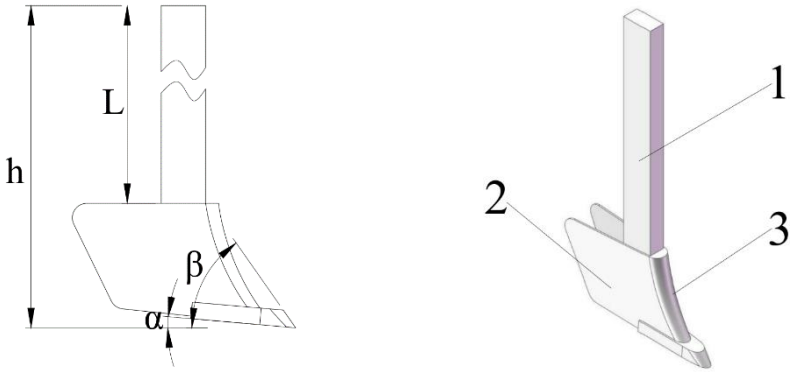


**Fig. 1 - Structure parameter diagram of furrow opener**

*1 – Shovel handle; 2 – Retaining plate; 3 – Cutting edge*

*h: Height of the furrow opener; L: Length of the shovel handle; α: Rake angle; β: Penetration clearance angle*

**Site and equipment description**

The indoor experiment was carried out in the laboratory of the Conservation Tillage Innovation Team, Shandong University of Technology. The soil bin test bench with control the system for adjusting parameters was used to analyze ditching experiment, and the structure of the soil bin test bench was designed by Conservation Tillage Innovation Team (Fig. 2b). The soil bin test bench was mainly composed of frame, mobile device, lifting device and control system. The mobile device adopted the form of sliding block and linear cylindrical guide rail to realize the linear movement of the device. The lifting device, mounted on the moving beam, controlled the ball screw through the stepper motor to achieve the upper and lower displacement of the sliding table. The control system was mainly composed of intelligent serial screen, Arduino controller, photoelectric limit switch sensor and speed encoder. The technical parameters of the soil bin test bench were shown in Table 1.

Input the corresponding control signal to the control the system through the touch screen, and transmitted the obtained signal to the stepper motor driver to control the stepper motor to rotate forward and reverse at the expected speed. At the same time, the stepper motor transmitted the power to the moving beam through the sprocket-chain mechanism, which drove the moving beam to move horizontally along the cylindrical guide rail. The lifting system was mounted on the moving beam and moved laterally with the moving beam, and the mounting plate of the tillage parts on the lifting system moved up and down with the movement of the ball screw mechanism. The control signal can control the rotation of the motor at the top of the lifting system, which in turn drove the mounting plate of the tillage component to move up and down with the ball screw mechanism to realize the adjustment of the working depth. The schematic diagram of the control system was shown in Fig. 2c.

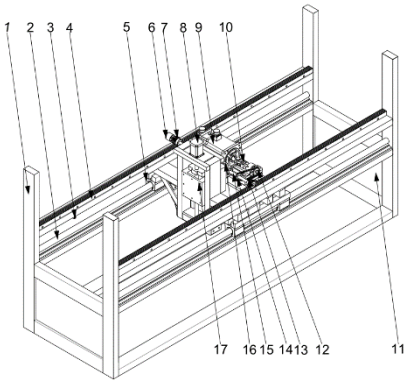


(a) Schematic diagram of soil bin structure

(b) Actual diagram of soil bin structure

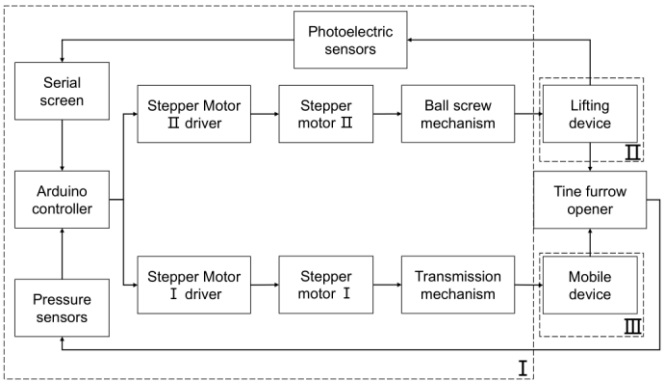


(c) Schematic diagram of the control system

**Fig. 2 - Soil bin test bench**

*1 – Frame; 2 – Linear cylindrical guide; 3 – Photoelectric sensors; 4 – Rack; 5 – Slider; 6 – Speed encoder; 7 – Gear; 8 – Stepper Motor Ⅱ; 9 – Stepper Motor Ⅰ; 10 – Drive shaft Ⅰ; 11 – Acrylic sheet; 12 – Driving wheel; 13 – Chains; 14 – Driven wheel; 15 – Drive shaft Ⅱ; 16 – Bearing housing; 17 – Lifter; Ⅰ – Control system; Ⅰ –Mobile device; Ⅲ – Lifting device*

**Table 1**

**Technical parameters of test bench**

| Projects | Parameter |
|---|---|
| Machine size (m) | 8×1×1 |
| Horizontal velocity (m·s$^{-1}$) | 0-1.62 |
| Maximum traction (N) | 649 |
| Lifting displacement (mm) | 0-300 |
| Maximum lifting force (N) | 13572 |

There are different types of furrow opener arrangements. According to the different crops and the structure of the planter, the furrow openers were arranged on the planter in single-row (Fig. 3b) and multi-row configurations (Fig. 3a). In order to analyze the effect of furrow openers on soil disturbance and the interaction between multiple furrow openers, the position of the furrow openers needed to be adjusted during the trenching process.

In order to simulate the ditching process of no-tillage planter, the suspension bracket, made up of aluminum profiles and angular codes, were fixed on the lifting device, and the angular codes were used to connect aluminum profiles. Then the test tine furrow openers can be mounted on the suspension bracket by U-shaped bolt respectively. The suspension bracket, which may contain multiple beams according to experiment requirements, was shown in Fig. 3. Before the test, it was necessary to set the motion parameters (operation speed and operation depth) of the tillage parts through the touch screen according to the experimental design, and the position of each furrow opener needed to be installed according to the arrangement requirements.

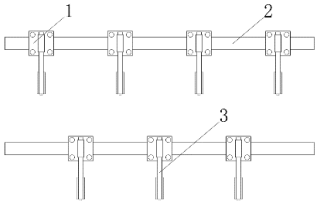


(a) Multi-row furrow opener layout

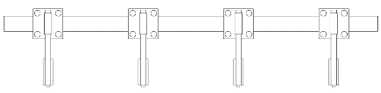

(b) Single-row furrow opener layout

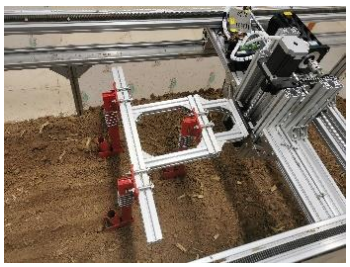

(c) Connection diagram of furrow opener

**Fig. 3 - Layout diagram of furrow opener**

*1 – Fixtures; 2 – Rack; 3 – Furrow opener*

During the experiment, in order to ensure that the soil parameters in the soil bin were close to the soil environment of the farmland, the tillage tool was used to loosen the soil and the soil was compacted. Then the appropriate amount of water was sprayed on the treated soil surface, and the ploughing tools were used to loosen the soil again when the water went deep into the soil. Each treatment was repeated three times before the ditching experiment. The soil texture in the soil bin was loam. The samples of test soil in soil bin were used to measure the moisture content by oven drying method and GZX-9146MBE dryer. The soil bulk density was measured by weight method. Soil aggregates analyzer (TPT-100) was used to measure the proportions of soil water-stable aggregates of the test soil by wet-sieving method. Soil conditions of the soil bin were included in Table 2.

**Table 2**

**Technical parameters of test bench**

| Soil type | Depth (cm) | Soil moisture content (%) | Soil dry bulk density ($g \cdot cm^{-3}$) | Proportions of soil water-stable aggregates | | | | |
|---|---|---|---|---|---|---|---|---|
| | | | | > 5 mm | 5-2 mm | 2-1 mm | 1-0.5 mm | <0.5 mm |
| Loam | 0-3 | 11.36 | 1.258 | 12.3 | 23.6 | 22.4 | 30.5 | 11.2 |
| | 3-6 | 14.57 | 1.274 | 10.2 | 32.5 | 14.6 | 27.5 | 15.2 |
| | 6-10 | 17.13 | 1.293 | 9.98 | 27.8 | 29.7 | 23.4 | 9.12 |

When the speed of the seeder is too large, the operating performance of the seed rower will be reduced *(Ballel.Z., Moayad, 2009; Liu et al., 2009; Yao et al., 2007)*. In order to ensure the stability of the seed rower, the operating speed selected for this test was 1 m/s, and the operating speeds of 0.8, 1.2 m/s were selected as the control experiment. According to the agronomic requirements *(Wang, 2014)*, the trenching depth of this experiment was 50 mm, and the trenching depth of 100 mm was selected as the control experiment. During the experiment, the OSG030 - 790UM high-speed camera, with the time resolution of 790 frames/s, was used to record the ditching process of the furrow opener. And the AMCAP software was used to obtain the dynamic video at a specific location. The high-speed camera was perpendicular to the forward direction of the furrow opener, and its layout was shown in Fig. 4. Kinovea software was used to post-process the recorded video to obtain the required image and analyze the disturbance behavior of the furrow opener on the soil during the trenching process.

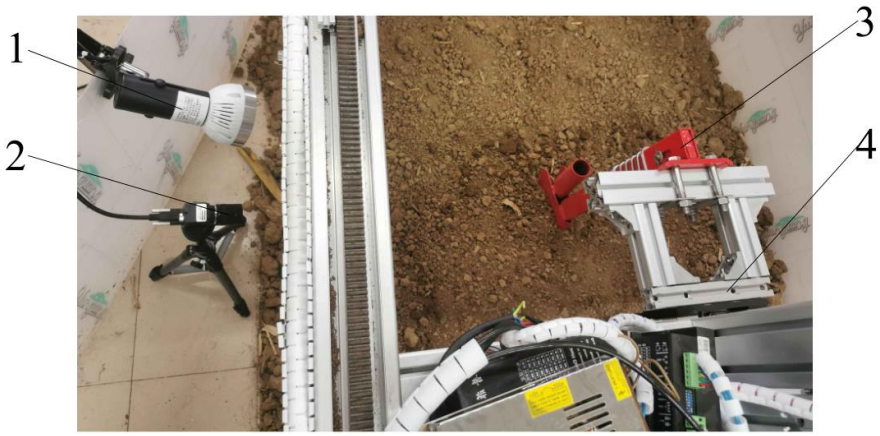


**Fig. 4 - Location and schematic of high-speed camera**

*1 – Fill light; 2 – High-speed camera; 3 – Furrow opener; 4 – Fixtures*

**Measurements**

After the ditching experiment, the measuring tool was used to measure the ridge height (*df*), soil dumping width (T), soil cutting width ($W_{fs}$), and operating depth (t) after tillage. In order to ensure the accuracy of the test data, the measurements of each ditching line were carried out at three positions, and the required data were obtained by calculating the average value. All the tests were replicated for five times.

The cross-sectional area (S) of seeding furrow type and the soil disturbance rate (D) can be used as evaluation indexes to analyze the effect of furrow opener on soil disturbance. After the end of the soil bin test, soil cutting width ($W_{fs}$), operating depth (*t*), ridge height (*df*) and soil dumping width (T) were measured by using the ruler, as shown in Fig. 5.


**Fig. 5 - Soil disturbance parameters after soil ditching**

*T: Soil dumping width; df: Ridge height; t: Operating depth; W: Width of furrow opener; Wfs: Soil cutting width*

The cross-sectional area (S) of soil disturbance was calculated by formula (1)*(Manuwa et al., 2012; Zhang et al., 2016)*, and the soil disturbance rate (D) was calculated by formula (2)*(Yao et al., 2020)*

$$S=\frac{w+w_{fs}}{2}t \quad (1)$$

Where:

*S* is the cross-sectional area of furrow opener, cm$^2$; *W* is the width of furrow opener, cm; $W_{fs}$ is the width of soil, cm; *t* is the operating depth, cm.

$$D=\frac{W_{fs}}{d}\times 100\% \quad (2)$$

Where:

$D$ is the soil disturbance rate, %; $W_{fs}$ is the width of soil, cm; d is the row spacing between furrow openers, cm, here 4 cm is taken.

**Data analysis**

After the simulation of opening operation, soil cutting width ($W_{fs}$) and operating depth (t) were measured by the clipping function of the EDEM simulation software. Then, according to Eq. (1) and (2), the cross-sectional area (S) of soil disturbance and the soil disturbance rate (D) were calculated, respectively, and compared with the test data obtained from the soil bin test. The relative error between the simulation results and the test results was calculated, which was defined as the percentage of the absolute difference between the simulation results and the test results.

**Discrete element simulation test**

In order to ensure the feasibility of the simulation, the following assumptions were made for the simulation process:

(1) The actual soil was simplified to a sufficient number of particles and certain quality and parameters were given to the soil particles.

(2) Hertz-Mindlin (no slip) contact model was selected for particle contact model.

(3) Tillage process was the process of furrow opener acting on soil particles at a certain speed.

**Modeling of furrow opener**

According to the simplification principle of numerical simulation, the furrow opener was simplified to remove the components unrelated to the operating process. The 3D model of the furrow opener was designed using SolidWorks according to the scale of 1:1 (Fig. 1), and imported into the Geometry item of EDEM in .igs format. The material properties of the furrow opener were set as the material was 45 steel, the density was 7865 kg/m$^3$, Poisson's ratio was 0.3, and the shear modulus was 7.9×10$^{10}$Pa *(Gou et al.,2012)*.

**Soil particle modeling**

Because the smaller the simulated soil particles are, the slower the simulation speed is and the larger the computer memory is occupied, the soil particles in the simulation are generally much larger than the actual soil particles *(Gao et al., 2022; Mak et al., 2012; Yuan et al., 2021)*. In order to improve the accuracy of the simulation of soil particles, the soil particles with a radius of 5 mm were selected in this paper *(Wang et al., 2017)*. Hertz - Mindlin (no slip) contact model was set as the contact model between soil particles, the soil density was 2550 kg/m$^3$, the Poisson's ratio was 0.38, and the shear model was 1.0×10$^6$ Pa. The accumulation angle test of soil particles was carried out, as shown in Fig. 6. The simulated accumulation angle test used a steel pipe with a radius of 15 mm, which contained 5000 soil particles. The steel tube was moved vertically upward at a uniform velocity of 0.01 m/s *(Wang et al., 2020; Wang et al., 2017)*, the simulation ended when all

particles stopped moving. The soil accumulation angle was measured using the protractor function in the EDEM software, and the comparison with Fig. 6b showed that the simulated soil particles basically matched the soil parameters in the soil bin.

(a) Simulation test (b) Soil bin test

**Fig. 6 - Accumulation angle test**

## EDEM modeling

The contact parameters between soil particles and furrow opener were shown in Table 3 *(Fang et al., 2016; Ucgul et al., 2014; Yu et al., 2020)*. According to the operating condition of wheat no-till planter in the field and the requirement of simulation test, the virtual soil bin was established in EDEM. The basic size (length × width × height) of the soil bin was set as 2000 mm × 1000 mm × 130 mm, 350000 soil particles were generated. According to the proportion of the soil height of each layer, the number of soil particles in the surface layer, the shallow layer, the middle layer, the deep layer and the lower layer of the furrow opener were set to 60000, 60000, 60000, 60000 and 110000 respectively. The simulation time step was 20%, and the grid cell was 2.5 times of the minimum soil particle size. The established virtual soil bin simulation model was shown in Fig. 7.

**Table 3**

**Contact parameters of discrete element simulation**

| Parameter | Numerical value |
|---|---|
| Soil particle radius, R1 (mm) | 5 |
| Soil density, ρ (kg·m$^{-3}$) | 2550 |
| Soil Poisson's ratio, μ | 0.38 |
| Soil shear modulus, G (Pa) | $1.0\times10^{6}$ |
| Furrow opener density, $\rho_1$ (kg·m$^{-3}$) | 7865 |
| Furrow opener Poisson 's ratio, $\mu_1$ | 0.3 |
| Shear modulus of the furrow opener, $G_1$ (Pa) | $7.9\times10^{10}$ |
| Soil-soil recovery coefficient | 0.6 |
| Soil-furrow opener recovery coefficient | 0.6 |
| Soil - soil static friction coefficient | 0.6 |
| Static friction coefficient of soil-furrow opener | 0.6 |
| Soil-soil dynamic friction coefficient | 0.4 |
| Dynamic friction coefficient of soil – furrow opener | 0.05 |

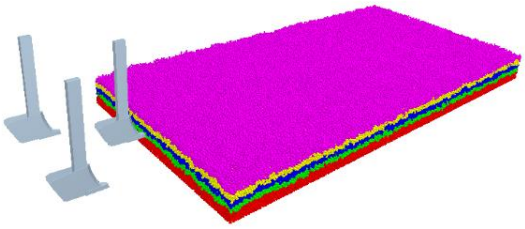

**Fig. 7 - Virtual soil bin model**

## RESULTS AND DISCUSSION

### Analysis of soil disturbance state

In order to analyze the disturbance behavior of soil particles at different depths, the soil was divided into five layers: the surface layer, the shallow layer, the middle layer, the deep layer and the lower layer of the furrow opener. Except the lower layer of the furrow opener, the depth of each layer was 25 mm, as shown in Fig. 8. In order to understand the disturbance behavior of the furrow opener on the soil during the trenching process, the forward direction and the vertical direction of the furrow opener were analyzed. Fig. 8a showed the longitudinal section of soil distribution, which was mainly used to analyze the disturbance behavior of soil caused by the furrow opener in the forward direction. Fig. 8b showed the transverse section of soil distribution, which was mainly used to analyze the disturbance behavior of soil caused by the furrow opener in the vertical forward direction.

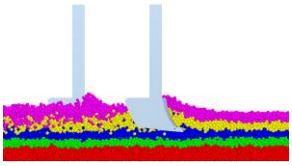
(a) Longitudinal section of soil distribution

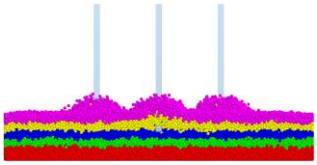
(b) Transverse section of soil distribution

**Fig. 8 - Soil distribution**

**Mechanism analysis of soil disturbance**

In the simulation process, the process of soil disturbance by the furrow opener was shown in Fig. 9. At 0.05 s, the front row furrow opener shovel tip completely entered the soil. At 0.22 s, the front row furrow opener completely entered the soil. At 0.3 s, the rear row furrow opener shovel tip completely entered the soil. At 0.47 s, the rear row furrow opener completely entered the soil. At 1 s, the front row furrow opener was in the middle of the trenching process. And at 1.25 s, the rear row furrow opener was in the middle of the trenching process.

It can be seen from Fig. 9 that in the trenching process of the furrow opener, the disturbance degree of the surface soil was the largest, followed by the shallow soil, followed by the middle soil, and the disturbance degree of the deep soil was the smallest. When the shovel tip of the furrow opener entered the soil (0.05, 0.3 s), the shallow soil and the middle soil started to move under the extrusion and shearing action of the shovel tip, respectively. The shallow soil pushed the surface soil upward to make it slightly elevated at the surface, while the middle soil moved downward to squeeze the deep soil and restrict its movement. When the furrow opener completely entered the soil (0.22 s, 0.47 s), under the cutting action of the furrow opener, the soil moved forward and upward with the furrow opener, expanding the longitudinal disturbance range of the soil. Under the pressing action of the retaining plate and the cutting edge, the soil moved forward with the furrow opener and moved to both sides, which increased the lateral disturbance range of the soil. As the furrow opener continued to work (1, 1.25 s), the shear force between the soils will reach the limit of the shear strength. At this time, the soil will undergo shear failure, and a fan-shaped soil fragmentation contour will be formed on the surface, and the contour will gradually expand to both sides along the direction perpendicular to the retaining plate as the furrow opener advanced. Based on the interaction between the shear effect of the cutting edge and the soil, the broken soil was further broken by the extrusion of the retaining plate. At this time, the movement of soil became more complex. Part of the soil moved forward and on both sides under the compression of the furrow opener, while the other part of the soil moved backward along the retaining plate through the friction with the furrow opener, and fell back to the ground under the action of gravity to backfill the seed trench. Comparing the disturbance of the front row and rear row furrow openers on the soil, it can be seen that at the same position, the disturbance behaviors of the front row and rear row furrow openers on the soil were basically the same.


0.05 s 0.22 s 1 s

**Fig. 9a - Soil disturbance process under high-speed camera**

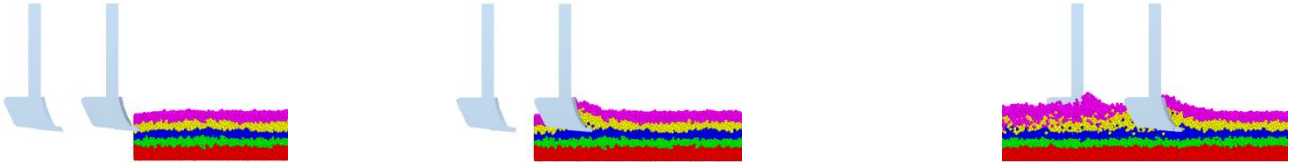
0.05 s 0.22 s 1 s

**Fig. 9b - Longitudinal disturbance section of the front row furrow opener**

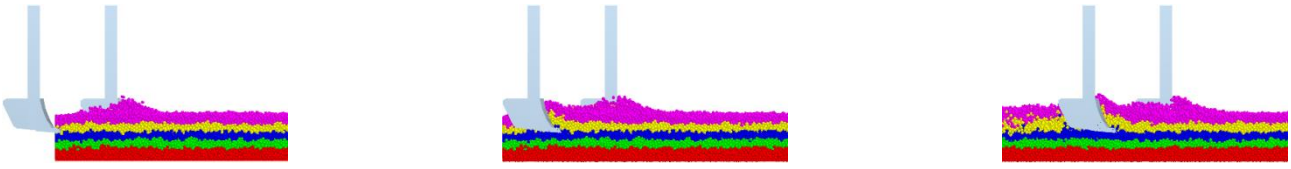
0.3 s 0.47 s 1.25 s

**Fig. 9c - Longitudinal disturbance section of the rear row furrow opener**

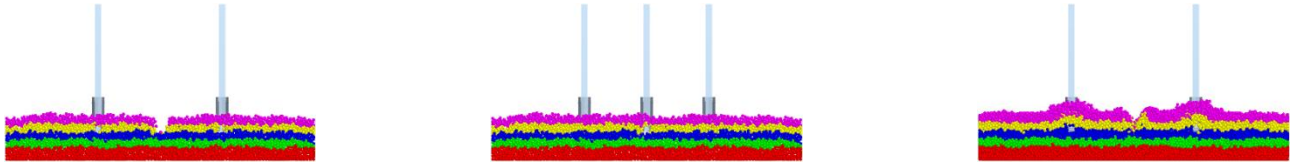


**Fig. 9d - Longitudinal disturbance section of the front row furrow opener**

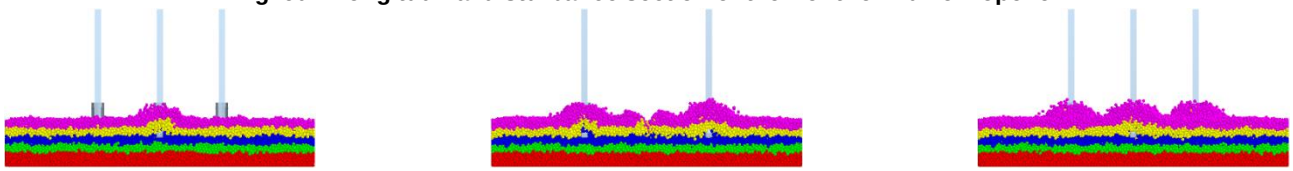


**Fig. 9e - Longitudinal disturbance section of the rear row furrow opener**

**Analysis of soil disturbance state at different positions**

In order to study the effect of the distance between adjacent furrow openers on soil disturbance, the soil at 1 s position was analyzed between horizontally and vertically (Fig.9). According to the disturbance of the soil in the transverse and longitudinal directions by the furrow opener, the 0 mm position of the profile was the transverse and longitudinal center of the front furrow opener. The longitudinal profile interval was 50 mm, and the transverse profile interval was 100 mm. The soil disturbance at different positions was shown in Fig.10.

It can be seen from Fig. 10a that the longitudinal disturbance degree of the furrow opener to the soil gradually decreased with the increase of the horizontal distance between the soil and the furrow opener. At the position 50 mm away from the furrow opener, the degree of soil disturbance gradually decreased, and the reduction degree of soil disturbance range was the lowest in the middle layer, followed by the shallow layer, and finally the surface layer. The degree of soil disturbance tended to stabilize at position 100 mm and above from the furrow opener. The main reason was that the influence of the soil by the force of furrow opener was decreased with the increase of the distance between the soil and the furrow opener.

It can be seen from Fig. 10b that the horizontal disturbance degree of the furrow opener to the soil gradually decreased with the increase of the longitudinal distance between the soil and the furrow opener. In the longitudinal center position of the furrow opener (0 m), the uplift of the soil by the furrow opener was small. At the center of the furrow opener shovel handle (100 mm), the soil was subjected to the pressing force and shearing force of the retaining plate, and was lifted to both sides along the forward direction of the furrow opener, which expanded the lateral disturbance range of the furrow opener. At the furrow opener tip position (200 mm), the soil received the strongest force from the tip, so the soil was lifted the most at this position. With the increasing distance between the soil and the furrow opener (300 mm), the amplitude of soil uplift gradually decreased. The main reason was that the squeezing and shearing effect of the furrow opener on the soil and the interaction between soil and soil were decreased with the increase of the distance between the soil and the furrow opener.

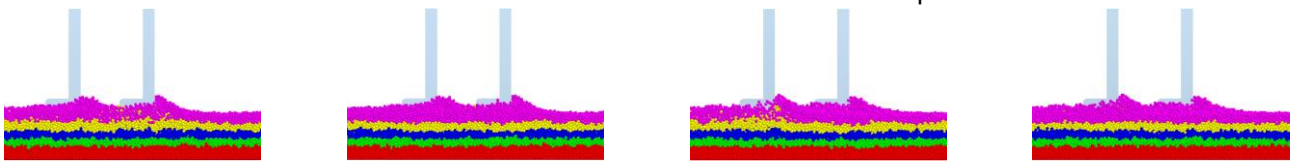


**Fig. 10a - Longitudinal disturbance section of the furrow opener**

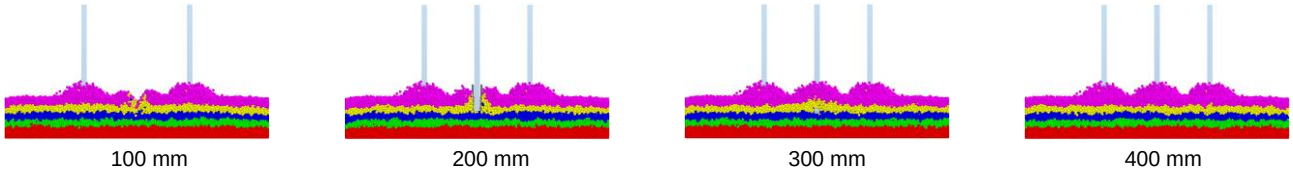


**Fig. 10b - Transverse disturbance section of the furrow opener**

*Analysis of soil disturbance state at different operating depths*

In order to analyze the soil disturbance caused by furrow opener under different operating depths, the soil disturbance of the furrow opener at 100 mm operating depth was selected for comparative analysis.

On the basis of Fig. 9, the soil at 1 s and 1.25 s was transversely and longitudinally examined to observe the disturbance of the front and rear furrow openers on the soil.

Fig. 11a showed that when the operating depth was 100 mm, the disturbance degree of the shallow soil was the largest, followed by the surface soil and the middle soil, and the deep soil was the smallest. The shallow soil was lifted upward by the squeezing action of the shovel handle, the shearing action of the cutting edge and the interaction between soil and soil, pushing the surface soil to move and making it slightly elevated at the surface. At the same time, the surface soil moved forward and upward under the squeezing action of the shovel handle, which increased the longitudinal disturbance range of the soil.

Fig. 11b showed that when the operating depth was 100 mm, the lateral disturbance range of soil was significantly larger than that when the operating depth was 50 mm. The main reason was that with the increase of the operating depth, the scope of action on the soil was also expanded. At this time, the soil was not only subjected to the shearing force of the cutting edge and the acting force between soil and soil, but also the shearing force and extrusion force of the shovel handle on the soil. The deep soil started to move under the squeezing and shearing action of the shovel tip. The downward movement of the deep soil squeezed the deep soil to restrict its movement, while the upward movement of the deep soil pushed the surface, shallow and middle soil to make it slightly elevated at the surface. Therefore, under certain conditions, the lateral disturbance range of soil will expand with the continuous increase of the depth of the furrow opener.

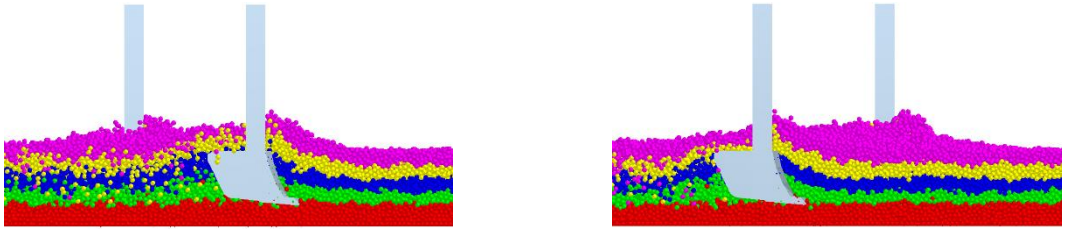


**Fig. 11a - Longitudinal disturbance section of the furrow opener**

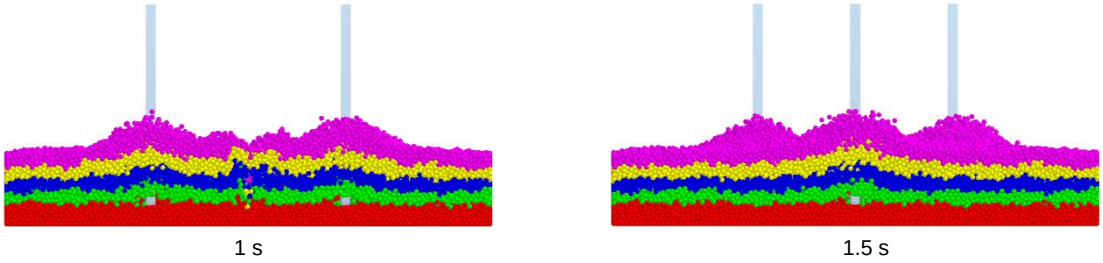


**Fig. 11b - Transverse disturbance section of the furrow opener**

*Analysis of soil disturbance state under different layouts*

In order to study the state of soil disturbance caused by the furrow opener under different arrangements, the arrangement modes of a single furrow opener and three furrow openers in parallel were selected. On the basis of Fig. 9, the soil at 1 s position was dissected laterally to observe the disturbance state of soil caused by the furrow opener.

It can be seen from Fig. 12a that ridge height was lower than that in Fig. 9e when only a single furrow opener was used. The main reason was that when a single furrow opener was used for trenching operation, the soil will only be subjected to the squeezing and shearing action of the furrow opener and the interaction between soil and soil, and will not be affected by other furrow openers, so the soil will be lifted to a lesser extent.

It can be seen from Fig. 12b that the ridge height was higher than that in Fig. 9e when three furrow openers were parallel. The main reason was that when the three furrow openers were in parallel, the soil was not only subjected to the extrusion and shear of the furrow opener and the interaction between soil and soil, but also subjected to the extrusion of the adjacent furrow openers, which made the soil lifted to a larger extent.

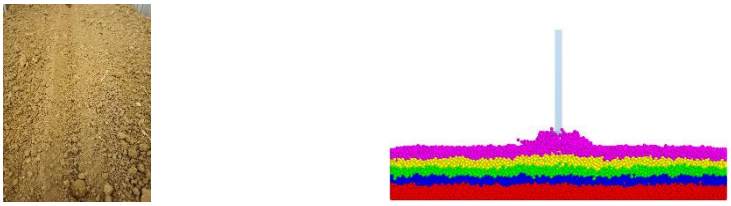

**Fig. 12a - The disturbance of single furrow opener on the soil**

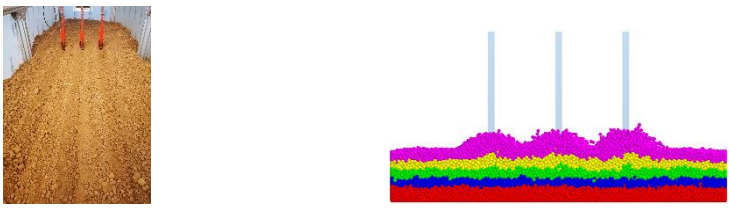

**Fig. 12b - Disturbance of parallel furrow openers on the soil**

**Analysis of soil movement state**

*Analysis of soil overall movement state by furrow opener*

In order to study the influence of the furrow opener on the soil movement state under different depths at different times, three positions were selected to analyze the movement velocity at different moments: the furrow opener tip into the soil (0.05, 0.3 s), the furrow opener completely into the soil (0.22, 0.47 s) and the furrow opener located in the middle of the trenching process (1, 1.25 s).

According to the color distribution of Fig. 13a, the middle soil moved forward and upward under the action of the shovel tip when the shovel tip entered the soil, and the surface soil and the shallow soil were lifted upward under the action of the middle soil. At this time, the velocity of the middle soil was the fastest, followed by the shallow soil, and least in the surface soil. When the furrow opener completely entered the soil, the soil particles with movement velocity were the most in the surface layer, followed by the shallow layer and the least in the middle layer. The closer the soil was to the furrow opener, the greater the velocity of movement, and the distribution curves of the same-speed soil particles were basically consistent with the curves of the furrow opener. At this time, the shallow soil and the middle soil were rose upward along the direction perpendicular to the shovel tip and the cutting edge. Under the extrusion and cutting action of the furrow opener and the disturbance of the shallow soil and the middle soil, the surface soil moved forward and upward. When the furrow opener was in the middle of the trenching process, the movement of the soil in front of the furrow opener was not much different from that when the furrow opener was completely in the soil. When the soil moved forward, it was also moved backward along the retaining plate through friction with the furrow opener, and fell back to the ground under the action of gravity to backfill the seed trench. As can be seen from Figure 13b, the movement of the soil during tillage of the rear row furrow opener was basically the same as the tillage process of the front row furrow opener.

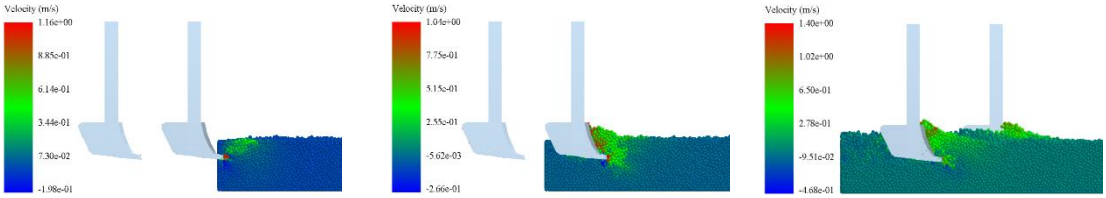


0.05 s 0.22 s 1 s

**Fig 13a - Analysis of the whole movement state of soil by front row furrow opener**

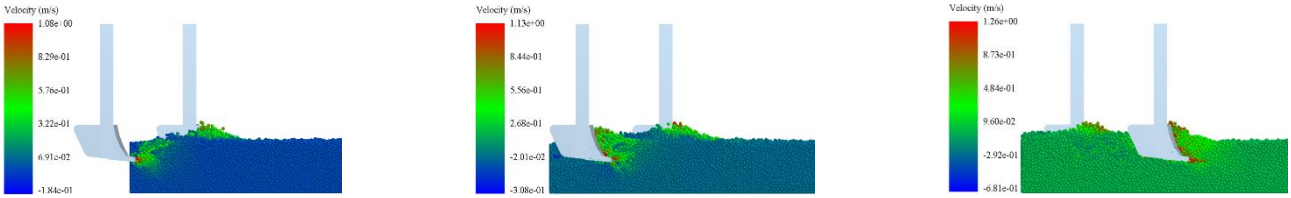


0.3 s 0.47 s 1.5 s

**Fig 13b - Analysis of the whole movement state of soil by rear row furrow opener**

**Analysis of soil particle motion at different velocities**

In order to analyze the movement state of each soil layer under different speeds of furrow opener, the operating speeds were selected as 0.8, 1 and 1.2 m/s to obtain the average horizontal, vertical and lateral speeds of the surface layer, the shallow layer and the middle layer, as shown in Fig. 14.

It can be seen from Fig. 14 that during the ditching process, the average velocities of soil at different depths were varied with the advance of the furrow opener. When the operating speed was 0.8 m/s, in the x-direction, the average velocities of the surface layer, the shallow layer and the middle layer were 0.010216, 0.006969 and 0.002948, respectively. In the y-direction, the average velocities of the surface layer, the shallow layer and the middle layer were 0.00135, 0.001133 and 0.000617, respectively. In the z-direction, the average velocities of the surface layer, the shallow layer and the middle layer were 0.003678, 0.001867 and 0.000799,

respectively. When the operating speed was 0.8 m/s, the average speeds from large to small were the surface layer, the shallow layer and the middle layer (Fig. 14a). When the operating speed was 1 m/s, in the x-direction, the average velocities of the surface layer, the shallow layer and the middle layer were 0.014108, 0.008219 and 0.003365, respectively. In the y-direction, the average velocities of the surface layer, the shallow layer and the middle layer were 0.0012896, 0.000995 and 0.000856, respectively. In the z-direction, the average velocities of the surface layer, the shallow layer and the middle layer were 0.004341, 0.002103 and 0.000807, respectively. When the operating speed was 1 m/s, the average speeds from large to small were the surface layer, the shallow layer and the middle layer (Fig.14b). When the operating speed was 1.2 m/s, in the x-direction, the average velocities of the surface layer, the shallow layer and the middle layer were 0.01808, 0.01052 and 0.003596, respectively. In the y-direction, the average velocities of the surface layer, the shallow layer and the middle layer were 0.001658, 0.001353 and 0.000868, respectively. In the z-direction, the average velocities of the surface layer, the shallow layer and the middle layer were 0.005327, 0.00286 and 0.001222, respectively. When the operating speed was 1.2 m/s, the average speeds from large to small were the surface layer, the shallow layer and the middle layer (Fig. 14c). At the same speed, the velocities of soil particles at different depths were different due to the extrusion, shear and interaction between soil and soil. As the operating speed of the furrow opener changed, the speed of the soil at the same depth in different directions will change accordingly.

It can be seen from Fig. 14 that the average velocities of the soil particles changed rapidly after the front row of furrow opener was completely inserted into the soil, and then tended to stabilize. In the x-direction, the average velocities of the surface layer, the shallow layer and the middle layer were significantly different, with the surface soil velocity being the largest, followed by the shallow soil, and the middle soil being the smallest. In the y-direction, the variation curves of average velocities of the surface layer, the shallow layer and the middle layer were basically the same. In the z-direction, the average velocities curves of the surface layer, the shallow layer and the middle layer were basically the same, and the change of the surface soil velocity was the most obvious.

The movement speeds of soil were analyzed under different times, different depths and different speeds. When the operating speed was 0.8 m/s, in the x-direction, the movement speed of the middle soil was the largest, while the movement speed of the shallow soil was slightly lower than that of the middle soil, and the movement speed of the surface soil was the smallest. In the y-direction, the movement speed of the shallow soil was the largest, and the difference between the movement speed of the surface soil and the middle soil was small. In the z-direction, the movement speed of the surface soil was the largest, and the difference between the movement speed of the shallow soil and the middle soil was small. When the operating speed was 1 m/s, in the x-direction, the movement speed of the shallow soil was the largest, and the difference between the movement speed of the surface soil and the middle soil was small. In the y-direction, the movement speed of the shallow soil was the largest, and the difference between the movement speed of the surface soil and the middle soil was small. In the z-direction, the movement speed of the middle soil was the largest, while the movement speed of the shallow soil was slightly lower than that of the middle soil, and the movement speed of the surface soil was the smallest. When the operating speed was 1.2 m/s, in the x-direction, the movement speed of the middle soil was the largest, the movement speed difference between the surface and the middle soil was small, and the movement speed of the shallow soil was the smallest. In the y-direction, the movement speed of the shallow soil was the largest, the movement speed difference between the shallow and the middle soil was small, and the movement speed of the surface soil was the smallest. In the z-direction, the movement speed of the middle soil was the largest, and the movement speed difference between the surface and the shallow soil was small, and the movement speed of the shallow soil was the smallest.

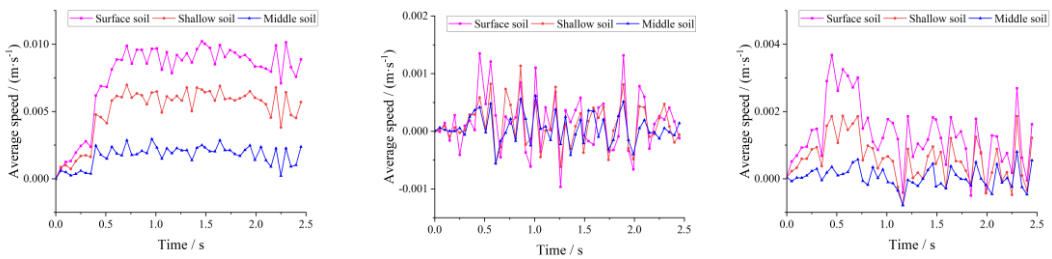


Average velocity in x-direction Average velocity in y-direction Average velocity in z-direction

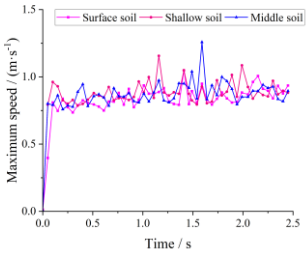


Maximum velocity in x-direction

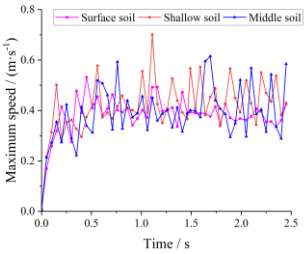


Maximum velocity in y-direction

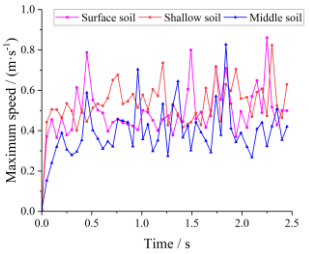


Maximum velocity in z-direction

(a) Operating speed of 0.8 m/s

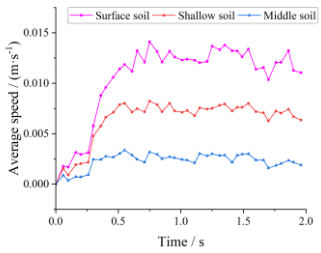


Average velocity in x-direction

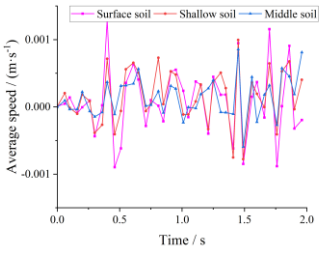


Average velocity in y-direction

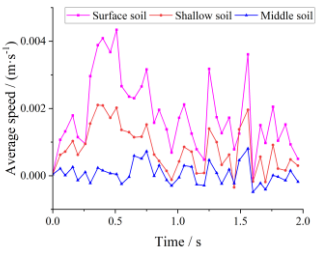


Average velocity in z-direction

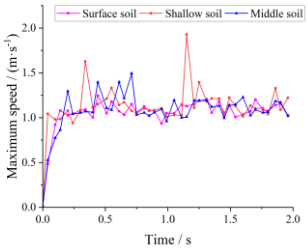


Maximum velocity in x-direction

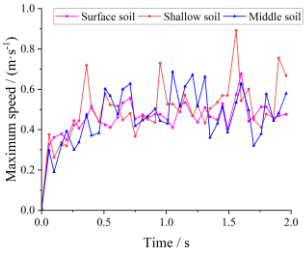


Maximum velocity in y-direction

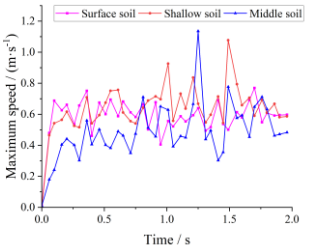


Maximum velocity in z-direction

(b) Operating speed of 1 m/s

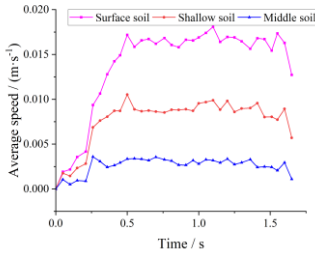


Average velocity in x-direction

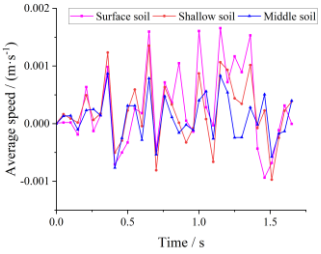


Average velocity in y-direction

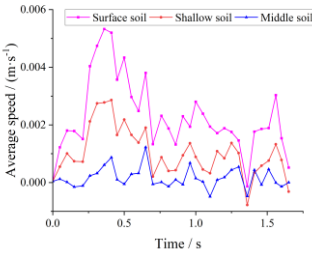


Average velocity in z-direction

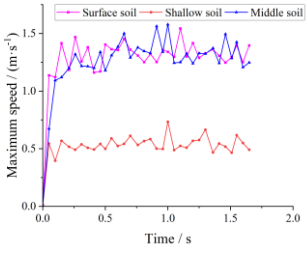


Maximum velocity in x-direction

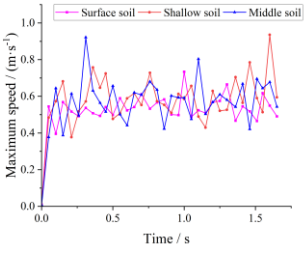


Maximum velocity in y-direction

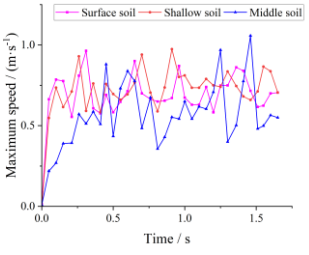


Maximum velocity in z-direction

(c) Operating speed of 1.2 m/s

**Fig. 14 - Movement speed of soil at different speeds and depths**

**Analysis of soil disturbance effect**

The data obtained from simulation and soil bin test were calculated separately, and the relative errors between the simulation and test results were calculated, as shown in Table 4.

**Table 4**

**Soil disturbance effect analysis**

| Parameter | Front row simulation value | Front row test value | Relative error (%) | Rear row simulation value | Rear row test value | Relative error (%) |
|---|---|---|---|---|---|---|
| Ridge height (cm) | 1.99 | 2 | 0.5 | 1.99 | 2.05 | 2.93 |
| Dumping width (cm) | 15.71 | 16.01 | 1.87 | 18.08 | 18.87 | 4.19 |
| Cutting width (cm) | 11.17 | 11.2 | 0.27 | 13.13 | 13.84 | 5.13 |
| Operating depth (cm) | 3.42 | 3.5 | 2.29 | 4.64 | 4.7 | 1.28 |
| Cross-sectional area ($cm^2$) | 25.94 | 26.6 | 2.48 | 39.74 | 41.92 | 5.2 |
| Soil disturbance rate (%) | 27.93 | 28 | 0.25 | 32.83 | 34.6 | 5.12 |

It can be seen from Table 4 that the experimental data of soil disturbance parameters, such as ridge height, soil dumping height, soil cutting height, operating depth and cross-sectional area of furrow opener, were slightly larger than the simulation data. Among them, the relative error of the cross-sectional area of the rear row furrow opener was the largest, which was 5.2%, and the relative error of the soil disturbance rate of the front row trench opener was the smallest, which was 0.25%. It showed that the simulation results can accurately reflect the disturbance of the soil during the trenching process of the furrow opener.

It can be seen from Table 4 that the parameters of the front row furrow openers were smaller than those of the rear row furrow openers. The reason may be that during the trenching process of the rear furrow openers, the soil moved to both sides under the action of the retaining plate, and filled back the seed furrow cultivated by the front row furrow opener under the action of gravity, making the data of the seed furrow cultivated by the front row furrow opener smaller. The disturbance process of the furrow opener to the soil provided a way of thinking about the layout of the furrow opener.

## CONCLUSIONS

(1) The macro-disturbing mechanism and micro-disturbing state of soil in trenching process were analyzed by combining discrete element simulation with high-speed camera and soil bin test. The range of soil disturbance decreased with the increase of the distance between the soil and the furrow opener, and the range of soil disturbance at different locations from large to small was the surface layer, the shallow layer and the middle layer. The degree of soil disturbance by the furrow opener varied at different operating depths. At the operating depth of 50 mm, the degree of soil disturbance from large to small was the surface layer, the shallow layer and the middle layer. At the operating depth of 100 mm, the degree of soil disturbance from large to small was the shallow layer, the surface layer, the middle layer and the deep layer. Through the test comparison of three different layout methods of furrow openers, it can be seen that taking the layout of interlocking furrow openers was conducive to reducing the degree of soil disturbance, so determining a reasonable layout of furrow openers was conducive to reducing the disturbance effect of furrow openers on the soil.

(2) The velocity of soil movement gradually decreased with the increase of distance between the soil and the furrow opener, and the distribution curves of the same-speed soil particles were basically consistent with the curves of the furrow opener. The average velocities of the soil in different directions under different operating speed conditions were basically the same, from large to small was the surface layer, the shallow layer and the middle layer. At the same operating speed, soil particles under different depths were squeezed and sheared by the furrow opener, also the interactions between soil and soil were different, that resulted in the different movement speeds of soil particles. At the same depth of the soil, with the increase of the speed of the furrow opener, the speed in different directions also increased. Under different operating speed conditions, the maximum speed of soil in different directions was quite different.

(3) The discrete element simulation can accurately simulate the soil disturbance process in the trenching process. By comparing the test data obtained from simulation and test, it was found that the data obtained from simulation and test were basically consistent. The relative errors of the cross-sectional area of the front furrow opener and the rear furrow opener were 2.48% and 5.2%, respectively. The relative errors of the soil disturbance rate of the front furrow opener and the rear furrow opener were 0.25% and 5.12%, respectively.

**ACKNOWLEDGEMENTS**

This work was financially supported by the National Natural Science Foundation of China (Grant No. 51805300).

**REFERENCE**

[1] Abo-Elnor, M., Hamilton, R., & Boyle, J. T. (2004). Simulation of soil–blade interaction for sandy soil using advanced 3D finite element analysis [J]. *Soil and Tillage Research*, *75*(1): 61-73. https://doi.org/10.1016/s0167-1987(03)00156-9.

[2] Ballel.Z.Moayad. (2009). effects of biomimetic surface designs on furrow opener performance [j]. *journal of bionic engineering*, *6*(03): 280-289.

[3] Barr, J., Desbiolles, J., Ucgul, M., & Fielke, J. M. (2020). Bentleg furrow opener performance analysis using the discrete element method [J]. *Biosystems Engineering*, *189*: 99-115. https://doi.org/10.1016/j.biosystemseng.2019.11.008.

[4] Chen, Y., Munkholm, L. J., & Nyord, T. (2013). A discrete element model for soil–sweep interaction in three different soils [J]. *Soil and Tillage Research*, *126*: 34-41. https://doi.org/10.1016/j.still.2012.08.008.

[5] Fang, H. M., Ji, C. Y., Chandio, F. A., Guo, J., Zhang, Q. Y., & Arslan, C. (2016). Analysis of soil dynamic behavior during rotary tillage based on distinct element method (基于离散元法的旋耕过程土壤运动行为分析) [J]. *Transactions of the Chinese Society of Agricultural Machinery*, *47*(03): 22-28. https://kns.cnki.net/kcms/detail/11.1964.s.20160118.1043.008.html

[6] Fang, H. M., Ji, C. Y., Tagar, A. A., Zhang, Q. Y., & Guo, J. (2016). Simulation analysis of straw movement in straw-soil-rotary blade system (秸秆-土壤-旋耕刀系统中秸秆位移仿真分析) [J]. *Transactions of the Chinese Society of Agricultural Machinery*, *47*(01): 60-67. https://kns.cnki.net/kcms/detail/11.1964.s.20151113.1140.012.html

[7] Fielke, J. M. (1999). Finite element modelling of the interaction of the cutting edge of tillage implements with soil [J]. *Journal of Agricultural Engineering Research*, *74*(1): 91-101.

[8] Gao, Z. H., Shang, S. Q., Xu, N., & Wang, D. W. (2022). Parameter calibration of discrete element simulation model of wheat straw-soil mixture in Huang Huai Hai production area [J]. *INMATEH-Agricultural Engineering*, *66*(1): 201-210.

[9] Gou, W., Ma, R. C., Yang, W. Y., Fan, G. Q., Lei, X. L., Hui, K., & Yang, H. Z. (2012). Design of opener on no-till wheat seeder (小麦免耕播种机开沟器的设计) [J]. *Transactions of the Chinese Society of Agricultural Engineering*, *28*(S1): 21-25.

[10] Huang, Y. X., Hang, C. G., Yuan, M. C., Wang, B. T., & Zhu, R. X. (2016). Discrete element simulation and experiment on disturbance behavior of subsoiling (深松土壤扰动行为的离散元仿真与试验) [J]. *Transactions of the Chinese Society of Agricultural Machinery*, *47*(07): 80-88. https://kns.cnki.net/kcms/detail/11.1964.s.20160517.0944.002.html

[11] Jia, H. L., Meng, F. H., Liu, L. J., Shi, S., Zhao, J. L., & Zhuang, J. (2020). Biomimetic design and experiment of core-share furrow opener (芯铧式开沟器仿生设计与试验) [J]. *Transactions of the Chinese Society of Agricultural Machinery*, *51*(04): 44-49+77.

[12] Liu, L. J., Yang, X. J., Li, C. R., Liu, Y. C., & Liu, D. S. (2009). Design of 2BMG - 24 no-till wheat planter (2BMG-24 型小麦免耕播种机设计) [J]. *Transactions of the Chinese Society of Agricultural Machinery*, *40*(10): 39-43.

[13] Liu, R., Li, Y. J., Liu, C. X., & Liu, L. J. (2021). Design and experiment of shovel type wide seedling belt oat seeding furrow opener (铲式宽苗带燕麦播种开沟器设计与试验) [J]. *Transactions of the Chinese Society of Agricultural Machinery*, *52*(09): 89-96. https://kns.cnki.net/kcms/detail/11.1964.S.20210726.0948.004.html

[14] Mak, J., Chen, Y., & Sadek, M. A. (2012). Determining parameters of a discrete element model for soil–tool interaction [J]. *Soil and Tillage Research*, *118*: 117-122. https://doi.org/10.1016/j.still.2011.10.019.

[15] Manuwa, S. I., Ademosun, O. C., & Adesina, A. (2012). Regression equations for predicting the effect of tine width on draught and soil translocation in moderately fine textured soil [J]. *Journal of Environmental Science and Engineering B*, *1*(6B): 820-825.

[16] Matin, M. A., Fielke, J. M., & Desbiolles, J. M. A. (2014). Furrow parameters in rotary strip-tillage:

Effect of blade geometry and rotary speed [J]. *Biosystems Engineering*, *118*: 7-15. https://doi.org/10.1016/j.biosystemseng.2013.10.015.

[17] Singh, S., Tripathi, A., & Singh, A. K. (2016). Effect of furrow opener design, furrow depth, operating speed on soil characteristics, draft and germination of sugarcane [J]. *Sugar Tech*, *19*(5): 476-484. https://doi.org/10.1007/s12355-016-0499-x.

[18] Tagar, A. A., Changying, J., Adamowski, J., Malard, J., Qi, C. S., Qishuo, D., & Abbasi, N. A. (2015). Finite element simulation of soil failure patterns under soil bin and field testing conditions [J]. *Soil and Tillage Research*, *145*: 157-170. https://doi.org/10.1016/j.still.2014.09.006.

[19] Ucgul, M., Fielke, J. M., & Saunders, C. (2014). 3D DEM tillage simulation: Validation of a hysteretic spring (plastic) contact model for a sweep tool operating in a cohesionless soil [J]. *Soil and Tillage Research*, *144*: 220-227. https://doi.org/10.1016/j.still.2013.10.003.

[20] Ucgul, M., Fielke, J. M., & Saunders, C. (2015). Defining the effect of sweep tillage tool cutting edge geometry on tillage forces using 3D discrete element modelling [J]. *Information Processing in Agriculture*, *2*(2): 130-141. https://doi.org/10.1016/j.inpa.2015.07.001.

[21] Ucgul, M., Saunders, C., & Fielke, J. M. (2017). Discrete element modelling of tillage forces and soil movement of a one-third scale mouldboard plough [J]. *Biosystems Engineering*, *155*: 44-54. https://doi.org/10.1016/j.biosystemseng.2016.12.002.

[22] Wang, J., Jiang, K. L., Yu, F., Chen, Z. H., Yu, Y. J., & Lai, Q. H. (2021). The simulation design and experiment of reverse ditcher for small grain coffee cultivation based on discrete element method (基于离散元法的小粒咖啡种植逆转开沟器的仿真与设计) [J]. *Journal of Agricultural Mechanization Research*, *43*(01): 62-69. https://doi.org/10.13427/j.cnki.njyi.2021.01.012.

[23] Wang, J. Z., Sun, W., Wang, H. C., Zhang, H., & Liu, X. L. (2021). Research of long wing and sharp angle opener (尖角长翼型开沟器的研究) [J]. *Journal of Agricultural Mechanization Research*, *43*(11): 64-70. https://doi.org/10.13427/j.cnki.njyi.2021.11.012.

[24] Wang, L. M., Fang, S. Y., Cheng, H. S., Meng, H. B., Shen, Y. J., Wang, J., & Zhou, H. B. (2020). Calibration of contact parameters for pig manure based on EDEM (基于 EDEM 的猪粪接触参数标定) [J]. *Transactions of the Chinese Society of Agricultural Engineering*, *36*(15): 95-102.

[25] Wang, S. J. (2014). Analysis on advantages and techniques of wheat planting in Shandong Province (山东省小麦种植优势分析及技术探析) [J]. *Agricultural development and equipment*, (10) 110. https://kns.cnki.net/kcms/detail/32.1779.th.20141031.1611.096.html

[26] Wang, W. W., Song, J. L., Zhou, G. A., Pan, B. T., Wang, Q. Q., & Chen, L. Q. (2022). Simulations and experiments of the seedbed straw and soil disturbance as affected by the strip-tillage of rowcleaner (Dem) [J]. *INMATEH Agricultural Engineering*, *66*(1): 49-61. https://doi.org/10.35633/inmateh-66-05.

[27] Wang, X. L., Hu, H., Wang, Q. J., Li, H. W., He, J., & Chen, W. Z. (2017). Calibration method of soil contact characteristic parameters based on DEM theory (基于离散元的土壤模型参数标定方法) [J]. *Transactions of the Chinese Society of Agricultural Machinery*, *48*(12): 78-85. https://kns.cnki.net/kcms/detail/11.1964.s.20170718.1412.026.html

[28] Yao, W. Y., Zhao, D. B., Xu, G. F., Chen, M. Z., Miao, H. Q., & Diao, P. S. (2020). Design and experiment of anti-blocking device for strip to row active corn no-tillage seeding (条带对行主动式玉米免耕播种防堵装置设计与试验) [J]. *Transactions of the Chinese Society of Agricultural Machinery*, *51*(S2): 55-62+71.

[29] Yao, Z. L., Gao, H. W., Li, H. W., & Wang, X. Y. (2009). Effect of different structural no-till openers on soil resistant force (不同结构免耕开沟器对土壤阻力的影响) [J]. *Journal of Agricultural Mechanization Research*, *31*(07): 30-34.

[30] Yao, Z. L., Gao, H. W., Wang, X. Y., & Li, H. W. (2007). Effect of three furrow openers for no-till wheat seeder on crop growth performance (小麦免耕播种机开沟器对作物生长的试验研究) [J]. *Transactions of the Chinese Society of Agricultural Engineering*, (07): 117-121.

[31] Yu, C. C., Wang, Q. J., Li, H. W., He, J., Lu, C. Y., & Liu, H. (2020). Design and experiment of spiral-split sowing strip cleaning device (螺旋切分式种带清理装置设计与试验) [J]. *Transactions of the Chinese Society of Agricultural Machinery*, *51*(S2): 212-219.

[32] Yu, J. Q., Qian, L. B., Yu, W. J., Pan, S. Q., Fang, Y., & Fu, H. (2009). DEM analysis of the resistances applied on furrow openers (开沟器工作阻力的离散元法仿真分析) [J]. *Transactions of the Chinese*

*Society of Agricultural Machinery*, *40*(06): 53-57.

[33] Yuan, P. P., Li, H. W., Jiang, G. J., He, J., Lu, C. Y., & Huang, S. H. (2021). Design and experiment of straw cleaning device for wide narrow maize no-tillage sowing strip in drip irrigation area (滴灌区宽窄行玉米免耕播种带秸秆清理装置设计与试验) [J]. *Transactions of the Chinese Society of Agricultural Machinery*, *52*(06): 43-52. https://kns.cnki.net/kcms/detail/11.1964.S.20210408.1333.009.html

[34] Zhang, R., Li, J. Q., Zhou, C. H., & Xu, S. C. (2007). Simulation of dynamic behavior of soil ahead of the bulldozing plates with different surface configurations by discrete element method (推土板表面形态对土壤动态行为影响的离散元模拟) [J]. *Transactions of the Chinese Society of Agricultural Engineering*, (09): 13-19.

[35] Zhang, X. C., Li, H. W., Du, R. C., Ma, S. C., He, J., Wang, Q. J., Chen, W. Z., Zheng, Z. Q., & Zhang, Z. Q. (2016). Effects of key design parameters of tine furrow opener on soil seedbed properties [J]. *International Journal of Agricultural*, *9*(3) 14.

[36] Zhao, S. H., Tan, H. W., Zhang, X. M., Liu, H. J., Cao, X. Z., & Yang, Y. Q. (2017). Design and numerical simulation of new acute angle opener (新型锐角开沟器的设计及数值模拟) [J]. *Journal of Agricultural Mechanization Research*, *39*(11): 44-48+58. https://doi.org/10.13427/j.cnki.njyi.2017.11.008.